Service Restoration of Coordinated Gas and Power Networks in Self-Healing Mode by Chance Constrained Adaptive Distributionally Robust Optimization

Navid Afsari, SeyedJalal SeyedShenava, and Hossein Shayeghi

***Abstract*—This article studies the role of coordination between a natural gas network and an electric power system in the optimal service restoration (SR) problem results. In the proposed coordinated model, the failure causes the upstream network's interruption, and the network's self-healing feature has been used for SR. The microgrid configuration changes are considered a variable and a choice for the operator. The SR problem faces some ambiguity in parameters due to the stochastic nature of electric vehicles and plug-in hybrid electric vehicles, as well as the availability and dispatching of natural gas-fired generation units, the ability to electric network reconfiguration, and the flexibility in demand response. Chance-constrained adaptive distributionally robust optimization (ADRO) is used to overcome these ambiguities of the uncertain parameters. A mixed-integer linear programming model is used for the problem, and the modified Civanlar test system is selected to evaluate the model. Besides ADRO, Stochastic Programming (SP), and ARO are applied to the model. In conclusion, SR in ADRO is 4% higher than SR in ARO owing to uncertainty realization in the worst possible way inside an uncertainty set. Also, SR for ex-ante protection is 19% lower than SP.**

***Index Terms*—Adaptive distributionally robust optimization (ADRO), dispatchable gas units, electric vehicles (EVs), gas network, service restoration (SR).**

NOMENCLATURE

Indices and Sets:

t, T	Index and set of the timeslots $[1 : N_t]$.
n, N	Index and set of the network nodes $[1 : N_n]$.
SN	State Number of the network topology $[1 : N_{SN}]$.
ω, Ω	Index and set of the scenarios $[1 : N_\omega]$.
b, B	Index and set of the electric vehicles' brand $[1 : N_b]$.
k, K	Index and set of the intervals in piecewise linearization $[1 : N_k]$.
xϵX	Feasible set of network structures.
i, I	Index and set of the NGFGUs $[1 : N_i]$.

Variables:

SR_i	Maximum service restoration in the *i*th structure.
$\mathbf{y}\epsilon\mathrm{Y}\ (\mathbf{x},\xi_\mathrm{F})$	Decision variables vector of the second stage.
$f^1(\mathrm{x}^1)$	Objective function of the optimization variables of the first stage.
$\mathbf{x^2}_{\xi\mathbf{1}}$	Results of the SR problem on the feasible set $\mathrm{X}^2(\xi^1)$.
$f^2(\mathrm{x}^1, \mathbf{x^2}_{\xi\mathbf{1}})$	Objective function corresponding to the vector of optimization variables of the second stage.
$\mathbb{E}_{\xi^1}\{z^1_{\xi^1}\}$	Expected value of the objective function associated to the variables in the second stage.
$\mathrm{P}^{\mathrm{b,n,t},\omega}_{\mathrm{CH-total}}$	Total charging power of the EV b, in the node n, at time t, and scenario ω.
$\mathrm{P}^{\mathrm{b,n,t},\omega}_{\mathrm{DCH-total}}$	Total discharging power of the EV b, in the node n, at time t, and scenario ω.
$\mathrm{P}^{\mathrm{b,n,t},\omega}_{\mathrm{EG-total}}$	Total EG output of the EV b, in the node n, at time t, and scenario ω.
$\mathrm{P}^{\mathrm{b,n,t},\omega}_{\mathrm{CH}}$	Charging power of the EV b, in the node n, at time t, and scenario ω.
$\mathrm{P}^{\mathrm{b,n,t},\omega}_{\mathrm{DCH}}$	Discharging power of the EV b, in the node n, at time t, and scenario ω.
$\mathrm{P}^{\mathrm{b,n,t},\omega}_{\mathrm{EG}}$	EG output of the EV b, in the node n, at time t, and scenario ω.
$SOC^{\mathrm{b,n,t},\omega}$	Operating SOC of the EV b, in the node n, at time t, and scenario ω.
η_ω, ζ	Auxiliary variables used in CVaR calculation.
$q_{l,t}$	Binary variable equals 1 if line l is closed.
$\xi_{j,t}$	Binary variable equals 1 if node j is a root node.
$f_{l,t}$	Artificial power flow on line l.
$\pi_\mathrm{n}/\pi_\mathrm{m}$	Nodal gas pressure.
fl_mn	Pipeline flow.

Constants and parameters:

ξ_F	Uncertain parameters corresponding to the weight coefficient of the load demands.
F ϵ D	Unknown but bounded distribution of the each element in the vector ξ_F.
$\mathbf{u}\epsilon$U	Variables associated with the weight coefficient of the load demands on the feasible set U.
η^b_{CH} , η^b_{DCH}	Charging and discharging of the EV b.
$SOC^\mathrm{b}_\mathrm{max}$	Maximum SOC of the EV b.
$SOC^\mathrm{b}_\mathrm{min}$	Minimum SOC of the EV b.
$\nu^\mathrm{max}_{sp}, \nu^\mathrm{min}_{sp}$	Max / min gas delivery of suppliers *sp*.

Received 4 February 2025; revised 8 September 2025; accepted 29 October 2025. Date of publication 25 November 2025; date of current version 14 January 2026. *(Corresponding author: Navid Afsari.)*

The authors are with the Department of Electrical and Computer Engineering, University of Mohaghegh Ardabili, Ardabil 56199-13131, Iran (e-mail: afsari-navid@gmail.com; seyedshenava@uma.ac.ir; hshayeghi@gmail.com).

Digital Object Identifier 10.1109/JSYST.2025.3628312

$L_l^{\max}, L_l^{\min}$	Max/min gas load.
a_g , b_g , c_g	Coefficients of the function of the EGs power generation.
A, B, C	Coefficients of the function of the natural gas consumption by NGFGUs.
$\lambda_E^{t,\omega}$	Demand values of the load type E at time t.
$\lambda_Q^{t,\omega}$	Demand values of the load type Q at time t.
$\lambda_G^{t,\omega}$	Demand values of the load type G at time t.
P_s^t	Probability of clearing the fault at time t.
ϕ_ω	Occurrence probability of scenario ω.
E^n	Size of the load type E in the node n(kW).
Q^n	Size of the load type Q in the node n(kW).
G^n	Size of the load type G in the node n(kW).
$\chi^{n,b}$	Number of the EV b, in the node n.
$U^{n,t,\omega}$	Statues indicator of the load type E where 1 means satisfied and 0 means shed.
$V^{n,t,\omega}$	Statues indicator of the load type Q where 1 means satisfied and 0 means shed.
$Y^{n,t,\omega}$	Statues indicator of the load type G where 1 means satisfied and 0 means shed.
$P_{NGFGU}^{i,t,\omega}$	NGFGU output of unit i, at time t, and scenario ω.
$F_{gas\_net}^{\mathrm{t},\omega}$	Total natural gas consumption at time t, and scenario ω.
$F_{gas}^{\mathrm{i,t},\omega}$	Natural gas consumption of unit i, at time t, and scenario ω.
ν_{sp}	Gas delivery amount of suppliers *sp*.
β	Risk weight}.
α	Confidence level.
$CVaR_\alpha$	CVaR with confidence level α.
τ	Availability factor of supplier1.
$\mathrm{n_b}$	Number of nodes in the distribution system.
M	Large constant.
$\mathrm{C_{mn}}$	Gas pipeline constant.

I. Introduction

A. Aim

RESEARCHERS have focused on the coordinated operation of electric power systems and natural gas networks due to the need for communication infrastructures and the availability of gas network information as a fuel for power grid generation units [1], [2]. The integration of these two systems is crucial for ensuring reliability and efficiency in the overall energy supply. By optimizing the coordination between electric power systems and natural gas networks, researchers aim to enhance the stability and resilience of the interconnected grid infrastructure.

Typically, the upstream network will feed loads in such a manner as to reduce operational costs while the system is in a normal operating state. As soon as a problem is detected, the network immediately begins the self-healing process. In order to restore load in the fault-affected regions, a flexible network operating in the self-healing mode can be provided by natural gas-fired generation units (NGFGUs), energy storage systems (ESSs), vehicle-to-grids (V2Gs), grid-to-vehicles (G2Vs), engine generators embedded in plug-in hybrid electric vehicles (PHEVs), as well as remote-control switches [3]. These technologies work together to quickly identify faults and automatically reconfigure the network to minimize downtime and maintain reliable power supply. By utilizing these advanced systems, grid operators can improve overall system resilience and minimize the impact of outages on customers.

B. Literature Review

Under the normal operating condition, the optimal operation schedule of distributed generations (DGs) in the microgrids (MGs) has been studied by researchers [4], [5]. On the other hand, resiliency, security, and reliability are the essential characteristics of the self-heal smart grids. The reason for the lack of a single standard for a self-healing network is because researchers are still learning about this subject. According to a National Energy Technology Laboratory assessment, self-healing is among the most important of the seven features of a modern grid [6].

Natural gas usage has grown exponentially in the recent decade as one of the most important fossil fuels, particularly for power production. Gas generators are expected to increase by more than 230% by 2030 [7], [8]. In this system, the gas network and the electricity network can exchange electric energy and natural gas, thus forming a multiple energy system [9]. In this condition, both electricity and natural gas networks should be operated simultaneously due to their interconnection in an economical way. In [10], the researchers analyzed the integration of gas pipelines with electricity distribution networks to improve overall system efficiency. In this article, a gas supply network is integrated with the IEEE-33 network, and the goal of optimal operation of this system is to use the conversion of natural gas into electricity to meet the load demand, considering the real-time price of electric energy in the upstream network.

In [11], the indirect effects of wind speed fluctuation and the effects of wind turbine output on the gas network have been studied through the mathematical model of the natural-gas price fluctuations with demand. In [12], an integrated power-gas-heat energy system nonlinear model coordinates the day-ahead schedule in the energy hub framework. The interconnection of electricity and natural gas systems is considered by a short-term stochastic model in [13]. In this article, a MILP model is applied for the coordinated natural gas and electricity systems, and the results are evaluated by considering the probability-based outages of transmission lines and generating units, as well as load forecast deviation.

In [14], an operational coordination optimization method is proposed for electricity and natural gas networks to overcome challenges in renewable energy generation. The method involves bidirectional energy flows through power-to-gas units and gas-fired power plants. The method is demonstrated in case studies, minimizing total operational cost, installed renewable energy generation curtailment, voltage imbalance, and overall carbon emissions.

The comparison of economic and environmental benefits of coordinated electricity and natural gas network planning to traditional independent planning, using piecewise linearization for efficient optimization, is evaluated in [15]. In [16], a risk-averse framework for optimizing an integrated power, gas, and electric vehicles (EVs) traffic network is provided, promoting social and environmental benefits and demonstrating its feasibility and effectiveness in various case studies.

C. Contribution

Emergency situations and network self-healing modes are not covered in the literature, despite the fact that it addresses how well natural gas and electric power networks coordinate

to operate as efficiently as possible. A mathematical model for the service restoration (SR) problem during the upstream network outage is presented in this article, allowing for optimal load restoration in the interaction between the electric power system and the gas supply network. The proposed model takes into account various constraints such as network capacity, demand, and operational costs to determine the optimal load restoration strategy. By incorporating gas and power network dynamics, this model provides a comprehensive approach to addressing emergency conditions and improving system resilience.

This article focuses on the optimal reconfiguration and operation of gas and power networks to increase the reliability and resilience of the system by maximizing SR. On the other hand, the load values as weighted coefficients are subject to uncertainty. The current problem has three dimensions. The first step is a planning strategy that is implemented prior to deciding on the MG configuration. The second level represents the most extreme realization of uncertainty when discussing uncertainty sets. The third level of the model illustrates the operational measures implemented to mitigate the undesirable consequences of uncertainty. As a result, it aims to increase the value of the objective function.

It is not necessary that the uncertain parameters be married to a strict probability distribution. They may, however, include some ambiguity regarding the probability distribution. ADRO is used to overcome these ambiguities of uncertain parameters. Along with NGFGUs and gas network dispatching, other evaluations include the program's ability to adjust and demand response in the presence of PHEVs and EVs, as well as their stochastic nature. A modified Civanlar test system is used to evaluate the model, and the problem is formulated as an MILP. Besides ADRO, stochastic programming and ARO are applied to the model.

Four case studies investigate the impact of solving method and dispatching in NGFGUs with EVs and PHEVs on SR problem analysis, verifying coordination between the electric power system and gas network. This study has made significant contributions, which include following.

1) The SR is maximized when MGs are isolated from the upstream grid, influenced by network capabilities such as reconfiguration, EV presence, and coordinated gas and electricity supply network operations.
2) Stochastic programming and robust optimization (RO) are two main methods for effectively dealing with uncertain parameters, which have also been used in this article. By incorporating ambiguity into the analysis, decision-makers can better understand the potential variability in outcomes in an unknown but bounded distribution and make more informed choices.
3) A nonanticipative concept is used to model the decisions by taking into account multistage classification for the different types of loads.
4) Plug-in hybrid EVs, load weights that are randomly assigned, demand response programs, and the gas system's coordinated operation are all taken into account simultaneously.
5) By comparing the ADRO response with ARO and Stochastic Programming (SP), it is clear that each method has a unique switching and optimal SR schedule, so the choice of the problem-solving method will be important.
6) Taking the ARO response as a basis, it can be concluded that by choosing ADRO, the optimal load recovery planning is protected from damage. On the other hand, the response obtained for SP can improve the SR plan, but it will not prevent significant damage from being incurred.

II. Formulation of Optimal Service Restoration Problem

The suggested robust and stochastic simulation model of SR incorporates the hourly optimal energizing schedule for controlling the interdependency of gas and power system constraints. This model takes into account uncertainties in both gas and power systems, providing a more realistic representation of the dynamic interactions between the two. The optimization model will optimize unit dispatching and energizing schedules to maximize SR while addressing natural gas and electricity constraints. Here is an illustration of the optimization model's framework

Max: Expected SR

s.t.

1) MGs, EVs, and NGFGUs constraints.
2) Hourly demand response constraints.
3) Fuel and natural gas network constraints.

A. Objective Function

In this SR problem, the objective function is the best hourly schedule of the MGs components, which includes NGFGUs, EVs, and PHEVs. It maximizes load restoration by considering technical constraints. In other words, to minimize the unsupplied customers, the SR problems can determine the restoration and operation program of the customers. Here, the objective function is maximizing the total weighted restored loads during the restoration as (1) shown at the bottom of this page.

B. MGs and Generator Units Constraints

1) Power Balance Constraint: Each MG's internal power balance is represented by

$$\sum_{N\in MG_i}\left(E^n U^{n,t,\omega}+Q^n V^{n,t,\omega}+G^n Y^{n,t,\omega}\right)\le \sum_{DG_i\in MG_i} P^{t,\omega}_{DG_i} + \sum_{P_{NGFGU,i}\in MG_i} P^{t,\omega}_{NGFGU_i} + \sum_{N\in MG_i}\left(P^{n,t,\omega}_{dch\_total}-P^{n,t,\omega}_{ch\_total}+P^{n,t,\omega}_{EG\_total}\right); \quad \forall n\in N\ \forall t\in T\ \forall\omega\in\Omega\ \forall i\in MG. \tag{2}$$

Based on this constraint, the total power generation of NGFGU sources and EV batteries, as well as the engine generator of the EVs in each MG, must be equal to the total

$$SR: \underset{U^{n,t,\omega},V^{n,t,\omega},Y^{n,t,\omega}}{Maximize} \sum_{\omega\in\Omega}\phi_\omega\left\{\sum_{t\in T} Ps_t\left(\sum_{n\in N}\left(\lambda^{t,\omega}_E E^n U^{n,t,\omega}+\lambda^{t,\omega}_Q Q^n V^{n,t,\omega}+\lambda^{t,\omega}_G G^n Y^{n,t,\omega}\right)\right)\right\}; \quad \forall n\in N\ \forall t\in T\ \forall\omega\in\Omega. \tag{1}$$

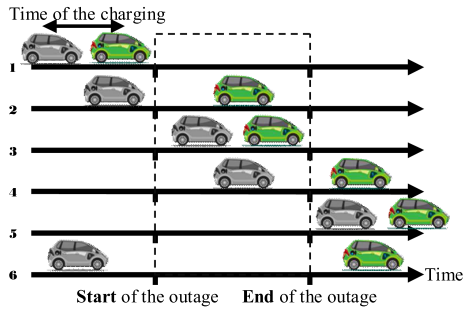

Fig. 1. Various scenarios according to present an EV in the parking lot during the outage.

partial restoration of the three types of responsive loads on each bus.

2) Charge/Discharge Constraints of the EVs: In this article, six possibilities depending on the start and end times of the outage, as well as the availability of an EV in the parking lot, are explored for the fault conditions represented in Fig. 1. These scenarios are classified based on the presence of the EV/PHEV in the parking lot during the emergence when the MGs are isolated from the main grid. The EV/PHEV uncertainty model includes: random SoC, fuel level for 8 brands, and the number of the present EVs during the fault, considering the parking lot's capacity [9].

Operational model of EV and PHEV with V2G and G2V capability has the charging/discharging schedule defined as follows:

$$0 \le P_{ch}^{\mathrm{b,n,t,\omega}} \le P_{CH-\max}^{b} \times \tau_{ch}^{\mathrm{b,n,t,\omega}}, \quad \forall b \in B\ \forall n \in N\ \forall t \in T\ \forall \omega \in \Omega \tag{3}$$

$$0 \le P_{dch}^{\mathrm{b,n,t,\omega}} \le P_{DCH-\max}^{b} \times \tau_{dch}^{\mathrm{b,n,t,\omega}}, \quad \forall b \in B\ \forall n \in N\ \forall t \in T\ \forall \omega \in \Omega \tag{4}$$

$$SOC_{\min}^{b} \le SOC^{b,n,t,\omega} \le SOC_{\max}^{b}, \quad \forall b \in B\ \forall n \in N\ \forall t \in T\ \forall \omega \in \Omega \tag{5}$$

$$SOC^{b,n,t+1,\omega} = SOC^{b,n,t,\omega} + (\tau_{ch}^{b,n,t,\omega} \times P_{ch}^{b,n,t,\omega} \times \eta_{ch}^{b} - \frac{\tau_{dch}^{b,n,t,\omega} \times P_{dch}^{b,n,t,\omega}}{\eta_{dch}^{b}})\Delta t\ \forall b \in B\ \forall n \in N\ \forall t \in T\ \forall \omega \in \Omega \tag{6}$$

$$\tau_{ch}^{b,n,t,\omega} + \tau_{dch}^{b,n,t,\omega} \le 1\ \forall b \in B\ \forall n \in N\ \forall t \in T\ \forall \omega \in \Omega \tag{7}$$

$$SOC_{arr}^{b,n,t,\omega} = SOC_{initial}^{b,n,t,\omega}\ \forall b \in B\ \forall n \in N\ \forall t \in T\ \forall \omega \in \Omega \tag{8}$$

$$SOC_{dep}^{b,n,t,\omega} = SOC_{final}^{b,n,t,\omega}\ \forall b \in B\ \forall n \in N\ \forall t \in T\ \forall \omega \in \Omega \tag{9}$$

Equations (10)–(11), which consider the discharge or charge power of each brand, the quantity of EVs from different brands, and the discharge/charge state of the binary control variable, calculate the total discharge and charge power of ESSs

$$P_{ch\_total}^{n,t,\omega} = \sum_{b \in B} \chi^{n,b} \times P_{ch}^{b,n,t,\omega} \times \tau_{ch}^{b,n,t,\omega}; \quad \forall b \in B\ \forall n \in N\ \forall t \in T\ \forall \omega \in \Omega \tag{10}$$

$$P_{dch\_total}^{n,t,\omega} = \sum_{b \in B} \chi^{n,b} \times P_{dch}^{b,n,t,\omega} \times \tau_{dch}^{b,n,t,\omega}; \quad \forall b \in B\ \forall n \in N\ \forall t \in T\ \forall \omega \in \Omega. \tag{11}$$

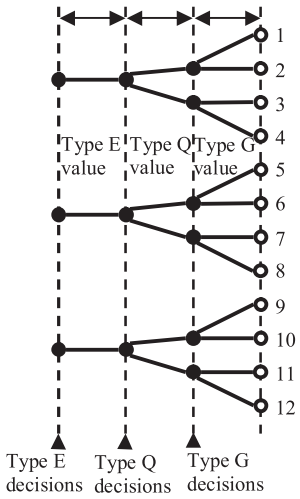

Fig. 2. Three-stage scenario tree of the load demand values: Type E, Type Q, Type G.

By multiplying two continuous and binary variables, these equations have a nonlinear form. The "big-M" approach is used to reform the problem in the MILP format and linearize this section of the problem [9], [17]. This model's big-M parameters are set to surpass the combined maximum discharge and charge power capacities of all EVs and PHEVs.

3) Engine Generators Embedded in PHEVs Constraint: An estimated curve and measured data can be used to create an example quadratic equation for an EG [18]. For example, (12) shows a relationship between the Chevrolet–Volt's output power and fuel consumption [19]. The fuel consumption during an hour, denoted by g(t), and the power generated by EG in an hour, denoted by P(g(t)), are represented as

$$P(g(t)) = -0.000105 \times g(t)^2 + 5.291 \times g(t) + 588.3;\ \forall t \in T. \tag{12}$$

This equation uses a linear piecewise function to approximate the nonlinear relation for each EG [9].

4) Uncertainty of Load Demand Values Based on Nonanticipativity: The nonanticipativity constraints of the example are detailed in [9] and [20]. In this reference, the details of the value of the load demands with the nonanticipative behavior are indirectly related to the financial issues of network operation.

The design of the scenario tree of the load demand values for this problem is shown in Fig. 2. For type E, type Q, and type G load values, respectively, the values of the vectors A^E, A^Q, and A^G are configured. The details of the scenario tree and establishing the vectors are presented in [20]. Vectors A^E and A^Q are presented in (13) and (14)

$$A^E = A^Q = [1,1,1,0,1,1,1,0,1,1,1,0]. \tag{13}$$

The vector of A^G is defined as

$$A^G = [1,0,1,0,1,0,1,0,1,0,1,0]. \tag{14}$$

To sort the load values in an increasing procedure for every scenario ω for type E and in each period t, nondecreasing value curves in the matrix O^E are expressed as

$$O^E = \begin{bmatrix} 1 & 1 & 1 & 1 & 2 & 2 & 2 & 2 & 3 & 3 & 3 & 3 \\ 1 & 1 & 1 & 1 & 2 & 2 & 2 & 2 & 3 & 3 & 3 & 3 \\ 1 & 1 & 1 & 1 & 2 & 2 & 2 & 2 & 3 & 3 & 3 & 3 \\ 1 & 1 & 1 & 1 & 2 & 2 & 2 & 2 & 3 & 3 & 3 & 3 \end{bmatrix}. \tag{15}$$

Furthermore, as demonstrated below, nonanticipativity constraints are used to ensure that the value of the load demands

does not decrease

$$U^{n,t,\omega} - U^{n,t,\omega'} \leq 0 \; \forall n \in N \; \forall t \in T \; \forall \omega \in \Omega;$$

$$O^E(t,\omega) + 1 = O^E(t,\omega'), \; if \; A^E(\omega) = A^E(\omega') = 0 \quad (16)$$

$$U^{n,t,\omega} - U^{n,t,\omega+1} = 0 \; \forall n \in N \; \forall t \in T \; \forall \omega \in \Omega;$$

$$\text{if } \mathrm{A^E}(\omega) = 1 \quad (17)$$

$$V^{n,t,\omega} - V^{n,t,\omega+1} = 0 \; \forall n \in N \; \forall t \in T \; \forall \omega \in \Omega;$$

$$\text{if } \mathrm{A^Q}(\omega) = 1 \quad (18)$$

$$Y^{n,t,\omega} - Y^{n,t,\omega+1} = 0 \; \forall n \in N \; \forall t \in T \; \forall \omega \in \Omega;$$

$$\text{if } \mathrm{A^G}(\omega) = 1. \quad (19)$$

Due to the hierarchical dependence of uncertainty, this problem takes into account nonanticipative uncertain scenarios. Here, scenarios are dependent on the conditions that were achieved in the preceding hour and are not independent over time. As demonstrated in this section, modeling nonanticipativity uncertainty adds complexity to the problem. However, in a real-world system, the scenarios may be independent and simple. As a result, solving the optimization problem in such conditions will be simpler, and according to experiments, the results obtained from optimizing the problem usually converge to a single answer, and there will be no variation in the answers.

5) General Connectivity Constraints: In this article, according to graph theory, the fundamental loops are used to reconfigure MGs. The network is represented as a graph equivalent. The details of the fundamental loop vectors are presented in [17] and [18]. The graph theory states that a radiant graph needs to meet two requirements: 1) each subgraph needs to ensure connectivity; 2) the number of edges must equal the number of nodes minus the number of subgraphs. The following constraints are used to formulate these two requirements [21]

$$\sum_{l \in N_l} q_{l,t} = n_b - \sum_{j \in R} \xi_{j,t} \; \forall t \in T \quad (20)$$

$$\sum_{l \in \delta(j)} f_{l,t} - \sum_{l \in \sigma(j)} f_{l,t} = 1 \; \forall t \in T \; \forall j \in N_b/R \quad (21)$$

$$1 - M\xi_{j,t} \leq \sum_{l \in \delta(j)} f_{l,t} - \sum_{l \in \sigma(j)} f_{l,t} \leq 1 + M\xi_{j,t} \; \forall t \in T, \; \forall j \in R \quad (22)$$

$$-Mq_{l,t} \leq f_{l,t} \leq Mq_{l,t} \; \forall t \in T \; \forall l \in N_l. \quad (23)$$

It is assumed that each fundamental loop contains a set of controllable switches. So, there are three fundamental loops in the studied network (C1–C3), as shown in Fig. 3. This modular design allows for flexibility and efficient management of the network's operations

$$FLV_1 = \{L_1, L_2, L_4, L_5, L_8, L_9, L_{11}, L_{17}\}$$
$$FLV_2 = \{L_2, L_3, L_8, L_{10}, L_{13}, L_{14}, L_{18}\}$$
$$FLV_3 = \{L_1, L_3, L_4, L_6, L_7, L_{13}, L_{15}, L_{16}, L_{19}\}.$$

C. Natural Gas System Constraints

1) NGFGU Generating Constraints: Physical constraint on capacity limits for each NGFGU power production is expressed as [13]

$$P^{\min}_{NGFGU_i} \leq P^{i,t,\omega}_{NGFGU} \leq P^{\max}_{NGFGU_i}; \; \forall t \in T \; \forall \omega \in \Omega \; \forall i \in I. \quad (24)$$

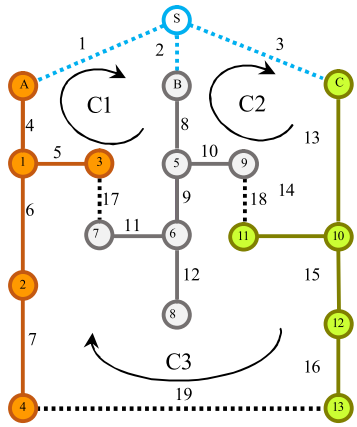

Fig. 3. Branch-node (Graph) model of the studied network.

2) Natural Gas Fuel Constraints: The hourly generation of NGFGUs is used to calculate natural gas consumption in (25). The natural gas network model categorizes the supply of NGFGUs as a natural gas load. On the other hand, the natural gas consumption by NGFGUs cannot exceed the capacity of the natural gas network

$$F^{\mathrm{i,t},\omega}_{gas} = A + BP^{\mathrm{i,t},\omega}_{NGFGU} + C\left(P^{\mathrm{i,t},\omega}_{NGFGU}\right)^2 \forall i \in I, \; \forall t \in T; \; \forall \omega \in \Omega \quad (25)$$

$$\sum_{i \in I} F^{\mathrm{i,t},\omega}_{gas} \leq F^{\mathrm{t},\omega}_{gas\_net}; \; \forall i \in I \; \forall t \in T \; \forall \omega \in \Omega. \quad (26)$$

The nonlinear relation of the natural gas consumption is approximated with the linear piecewise function to linear constraints in [9].

3) Natural Gas Supply and Load Constraints: There are similarities between gas and electricity systems. Both are designed to operate within reasonable ranges. The natural gas transmission system, one of the largest and most complex nonlinear systems, can be represented by its steady-state and dynamic operating characteristics [13]. In steady-state conditions, the extracted natural gas from each node equals the amount injected into the node. The gas delivery amount of suppliers *sp* restricted by its upper and lower limits and availability factors τ as

$$\begin{cases} A \leq \nu_{sp} \leq B \\ B = \nu^{\max}_{sp} \times \tau \\ A = \nu^{\min}_{sp} \end{cases}. \quad (27)$$

There are other potential categories of gas loads outside NGFGUs, including residential, commercial, and industrial. The gas load is constrained in the same ways that the maximum and minimum generating limitations of NGFGUs are

$$L^{\min}_l \leq L_l \leq L^{\max}_l. \quad (28)$$

The pipeline's parameters, such as its length, diameter, operating temperature, and pressure differential between its connected nodes, affect its flow. In a pipeline, the gas always moves from the higher-pressure node to the lower-pressure node. The model for the Weymouth equation is as follows:

$$fl_{mn} = \mathrm{sgn}(\pi_m, \pi_n) \; . \; C_{mn}\sqrt{|\pi^2_m - \pi^2_n|} \quad (29)$$

$$\operatorname{sgn}(\pi_m, \pi_n) = \begin{cases} 1, & \pi_m \geq \pi_n \\ -1, & \pi_m < \pi_n \end{cases} \tag{30}$$

$$\pi_m^{\min} \leq \pi \leq \pi_n^{\max}. \tag{31}$$

Actually, there is negligible loss in the flow in a single pipeline that is connected to the supply and load. This article, inspired by dc power flow, defines a linear relation for flow and Generation Shift Factor (GSF_{gas}) matrix to reflect the impact of nodal gas supply and load on the pipeline flow [22].

To evaluate the solution methods introduced for the SR, analysis and comparison of numerical results have been used in this section. The test systems' components are first presented. Then, the ability to dispatch in NGFGUs and the availability of the gas suppliers are evaluated using the ADRO. Also, SP and ARO are applied to the model, and the results are compared with ADRO. A linear structure expresses the mathematical model. The CPLEX solver is used to solve the model, which is implemented in GAMS as an MILP problem. Data entry and result presentation are done in the MATLAB environment, which is linked to GAMS by gdx.

III. Coordinated Natural Gas and Electric Power System Modeling With Robust and Stochastic Simulation

In this article, multistage classification is considered for the load types to generate scenarios. Also, changes in the MGs configuration are considered as a decision variable and a choice for the operator. There are two main methods for dealing with uncertain parameters. SP is a method that considers a large but limited number of uncertain parameters as scenarios [23]. The range of uncertain parameters is specified using sets or distribution bounds in RO [24]. A type of RO problem called Adaptive Distributionally Robust Optimization (ADRO) allows the user to make a decision before solving the optimization problem by taking into account the ambiguity of the uncertain parameters in an unknown range of the probability distribution function.

A. Tri-Level RO Model of Optimal SR Problem

When an upstream network failure occurs, the distribution network is separated into multiple sections. These sections can all be utilized as MGs since they can have storage and distribute generating resources. Based on these capacities, each subgrid needs to be able to restore the MG's maximum load. Here, this SR problem has a tri-level format for its objective function; the upper layer can determine the optimal network switching strategy until the fault is fixed. The restored loads are maximized at the lower level based on the load demand values. At the lower level, MGs with distributed power-generating sources, EVs, micro-generation turbines, and flexible loads address the optimum SR problem. Since there are two levels in the lower-level problem, tri-level solution techniques must be used. The upper level problem (UPPER) represents the high-level decision-making process, while the lower level monarch problem (LMP) focuses on optimizing the overall objective function. The lower level subproblem (LSP) is responsible for providing the inputs and constraints to the LMP, ensuring that it accurately reflects the system's behavior.

In the restoration process, a large number of 0/1 variables are added to the model because it involves optimal power dispatch and network reconfiguration. The suggested tri-level resilient optimization model corresponds to a large-scale MILP model.

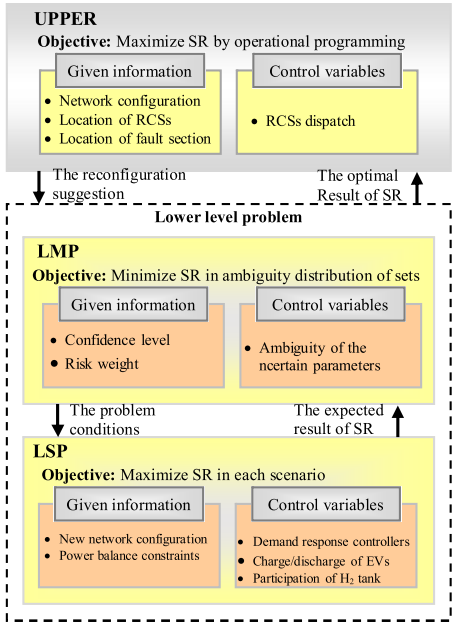

Fig. 4. Problems at the upper and lower levels.

The tri-level problem-solving process for optimal SR is also briefly shown in Fig. 4.

B. ADRO in SR Problem

In ADRO, each uncertain parameter is taken to follow an unknown bounded distribution. In fact, it is not practical to describe each parameter with a variable corresponding to the robust set. The model is as follows [25], [26]:

$$\max_{\mathbf{x}\in\mathcal{X}} \quad \min_{\mathcal{F}\in\mathcal{D}} \quad \max_{\mathbf{y}\in\mathcal{Y}(\mathbf{x},\boldsymbol{\xi}_{\mathcal{F}})} \quad \mathbb{E}_{\boldsymbol{\xi}_{\mathcal{F}}}\left\{f(\mathbf{x},\mathbf{y},\boldsymbol{\xi}_{\mathcal{F}})\right\}. \tag{32}$$

It is possible to violate the constraint because of the uncertainty of the uncertain parameters. A chance constraint is a probabilistic constraint that is physically involved in approximating these constraints [27].

1) Upper-Level Objective Function: The position of the fault, the controllable switches, the network architecture, and the placement of each MG's slack bus (generation unit) with frequency control are among the problem's upper-level inputs. During the restoration time, the upper-level objective function seeks the best SR program. The reconfiguration of the network and establishing power balance inside the reconfigured network are the constraints at this level. The constraints that are taken into account when forming the configuration of each MG for this purpose include the basic network structure, the location of the fault, the position of the controllable switches, and the buses connecting to the DG units with the ability to control the frequency using graph theory. The configuration of the newly created MGs updates the power balance constraint in each MG.

The formulation of the objective function and constraints at different levels of the problem is explained in Section II. The objective function will define the SR problem, while the constraints, such as general connectivity and radiality constraints and power balance at every MG, will limit the possible solutions to ensure they are feasible [28].

2) Lower-Level Objective Function: Lower-level optimization is used to address the SR problem and its parameter ambiguity caused by the stochastic nature of EVs and PHEVs, as well as

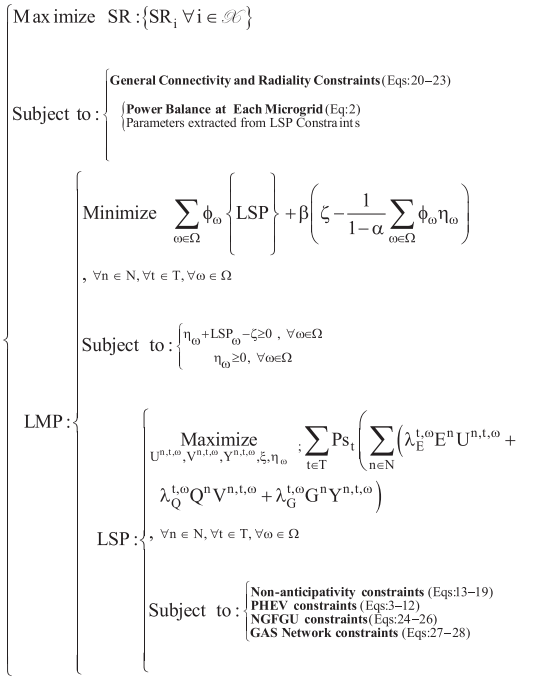

Fig. 5. Unified framework of the tri-level SR problem.

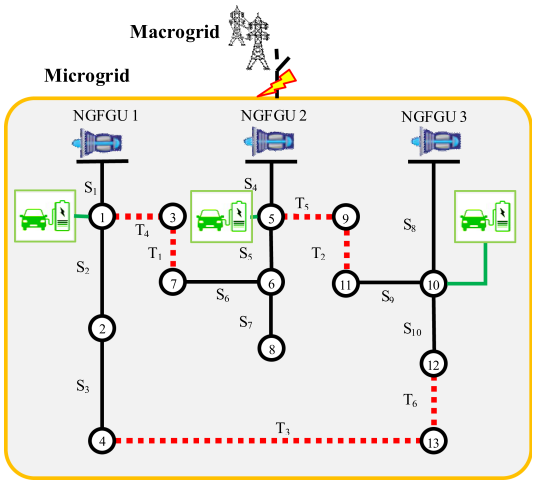

Fig. 6. Network configuration consisting of NGFGUs and parking lots.

the availability and dispatching of NGFGUs and the flexibility of demand response. The optimum SR issue's LMP takes the form of a conditional value-at-risk (CVaR) risk management problem. This approach allows for a more robust and efficient solution to the SR problem by considering the uncertainties and risks associated with various factors. By incorporating CVaR into the optimization framework, decision-makers can make more informed choices that prioritize reliability and cost-operational-effectiveness in SR planning.

The optimization problem in this article can be presented in a single format as Fig. 5.

The SR problem and its ambiguity in parameters due to the stochastic nature of EVs and PHEVs, as well as the availability and dispatching of NGFGUs, and the flexibility in demand response are optimized at lower level. The LMP for the optimal SR problem is formulated in the form of a risk management problem, specifically CVaR.

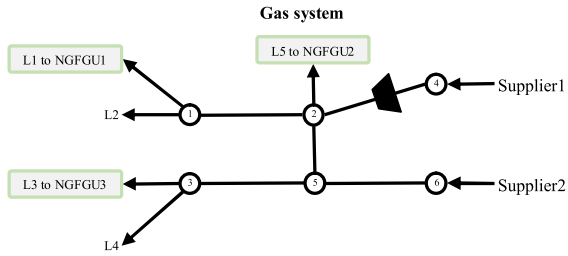

Fig. 7. Six-node natural gas system [13].

The value of the objective function at the LSP level is specified in the first section of the objective function in the LMP equation. The second term is related to risk management applied to the problem.

Maximization and minimization problems can be incorporated into the risk metric of CVaR when dealing with discrete scenarios. CVaR is the expected profit value below the $(1-\alpha)$-quantile, where $\alpha \in (0,1)$ is the scenario's confidence level, in a maximization problem, and the model maximizes the objective function with lower risk.

The CVaR criterion is the best method for evaluating ambiguity in sets, so it is used in this article even though it is more computationally complex than other approaches such as Bernstein and Wasserstein.

C. Adaptive RO in SR Problem

Often when uncertainty is realized, the inherent destructive effect of uncertainty may be reduced. This issue is included in the adaptive RO model. The problem of optimal SR in the coordination of the gas and electricity networks with the adaptive RO problem model has the following form:

$$\max_{\mathbf{x}\in\mathscr{X}} \quad \min_{\mathbf{u}\in\mathscr{U}} \quad \max_{\mathbf{y}\in\mathscr{Y}(\mathbf{x},\mathbf{u})} \quad f(\mathbf{x},\mathbf{y},\mathbf{u}). \tag{33}$$

An ARO problem consists of three levels. In general, Y is dependent on both **x** and **u** vectors.

D. Stochastic Programming in SR Problem

The problem of optimal SR in the coordination of the electricity and gas networks with the two-stage stochastic programming method has the following form [23], [29]:

$$\max_{\mathbf{x}^1\in\mathscr{X}^1} \quad f^1(\mathbf{x}^1) = \mathbb{E}_{\xi^1}\left\{z^1_{\xi^1}\right\},$$

$$\text{where}: z^1_{\xi^1} = \left\{ \max_{\mathbf{x}^2_{\xi^1}\in\mathscr{X}^2(\xi^1)} \quad f^2(\mathbf{x}^1,\mathbf{x}^2_{\xi^1}) \right\}. \tag{34}$$

IV. Computational Modeling of Self-Healing Gas and Power Systems

A. IEEE-13 Bus Power Network

The model described in Fig. 6 has been applied to the modified IEEE-13bus (Civanlar) network's island configuration [29]. In the presence of EVs as storage systems, this network has three NGFGUs with a nominal capacity of 80 kW. All three types of loads (E, Q, and G) are considered by each bus; their respective sizes are given in kW in [30]. Six tie-switches and ten lines connect the thirteen buses. Graph theory reconfiguration of this

network forms the matrix of fundamental loops in the same manner as that described in [31]. Three matrices will be created by matching the studied network with the branch-node model [19].

Uncontrollable factors include the quantity of electric cars in the parking lot at the time of the incident, the state of charge of the batteries, and the fuel level of the cars. Operating parameters of EVs are presented in [27]. Buses 1, 5, and 10 have parking lots nearby. Each brand has a limited quantity of electric cars; there are three of each brand's vehicles and 24 in the MGs. The number, charge state, and fuel level of EVs are assumed to follow random behavior.

B. Six-Node Gas Network

According to Fig. 7, the gas supply network consists of six buses that are fed from two nodes. Loads are connected to the network through three nodes. Gas loads connected to nodes 1, 2, and 3, respectively, are the fuel sources of the NGFGUs in buses 1, 5, and 10 in the power system network, in Fig. 6. The amount of these loads is determined based on the hourly production of NGFGUs. In addition, other gas consumers are also connected to nodes 1 and 3 named L2 and L4. Natural gas testing data adapted to this problem is presented in [32].

C. Basic Case Study

First of all, the network is considered to be unable to switch or reconfigure. Furthermore, the impact of EVs has been ignored. The NGFGU with continuous production (80, 80, 80, 80) kW sources starts to restore the loads when the upstream network is disconnected. This process lasts for 4 h until the upstream grid is connected again. During this time, the NGFGU operates in islanded mode to provide power to critical loads. In addition, the restoration process involves carefully balancing the available power sources with the demand to ensure a stable supply.

To evaluate the sensitivity of the problem to β, this parameter is gradually increased from 0 to 3, and the simulation is repeated. The confidence level is assumed to be $\alpha = 0.9$.

As β increases from 0 to 3, four individual responses are detected for the expected SR and CVaR. The locations of these variables are shown on a cumulative distribution function (PDF). The efficient curve for the problem can be created using PDFs of four optimization problem results as the efficient points, so the trend of variations in results for different β is shown in Fig. 8.

Details of the optimization results, including optimization results in 12 scenarios obtained from the scenario tree, and the expected value of the SR, as well as CVaR and value at risk (ζ), are presented in Table I. In this table, the results for β ranging from 0 to 3 are calculated for sensitivity analysis and are presented. The efficient Frontier's curve displays the trend of the optimization results' standard deviation decreasing from 45% to 26% as β increases. The CVaR result increases with an increase in β, which is an important advantage of the risk management tool.

The worst scenario in each β analysis has the most robustness across the solutions. Comparing the expected SR with CVaR (or VaR) for $\beta = \{0, 1, 2, 3\}$ reveals that employing the risk management tool improves the robustness of the solutions.

The characteristics of each MG's optimal SR schedule are shown in Fig. 9, including the 4-h steps until fault clearance for $\beta = 3$ and $\omega = 4$. The program outlines specific actions to be taken in order to restore service efficiently within the given time frame. It highlights the importance of quick response and effective coordination among MG components to minimize downtime and ensure a reliable power supply.

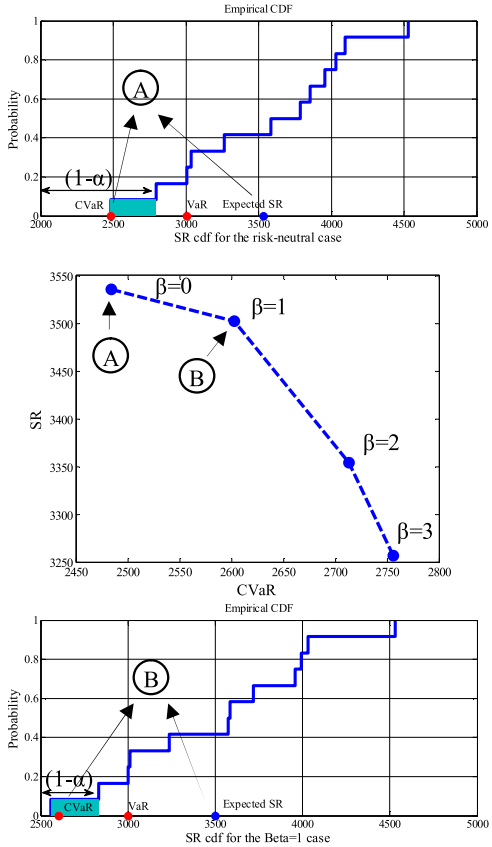

Fig. 8. Cdfs for $\beta = 0$ and $\beta = 1$ and SR versus CVaR (efficient Frontier).

TABLE I
RESULTS OF SR WITH VARIOUS βETA

	β=0		β=1		β=2		β=3	
	SR	η_ω	SR	η_ω	SR	η_ω	SR	η_ω
ω1	3788.6	0	3572.6	0	2934.3	0	2774.8	0
ω2	2797.1	0	2833.1	0	2805.3	0	2755.8	0
ω3	3036.1	0	3000.1	0	2972.3	0	2812.8	0
ω4	2484.6	0	2556.5	276.5	2695.3	110	2755.8	0
ω5	3854	0	3717.3	0	3534.1	0	3396.6	0
ω6	3264.6	0	3235.8	0	3219.1	0	3301.6	0
ω7	4094.6	0	3993.8	0	3644.1	0	3396.6	0
ω8	3005.6	0	3012.8	0	3107.1	0	3244.6	0
ω9	4529.3	0	4529.3	0	4074.2	0	3722.2	0
ω10	3955.8	0	3955.8	0	3778.2	0	3646.2	0
ω11	4029.8	0	4029.8	0	3852.2	0	3665.2	0
ω12	3585.8	0	3585.8	0	3630.2	0	3608.2	0
Expected SR	3535.5		3501.9		3353.9		3256.7	
CVaR	2484.6		2602.6		2713.6		2755.5	
ζ	2484.6		2833.1		2805.3		2755.5	
Lines opened	17-18-19 (#1) 17-18-19 (#2) 17-18-19 (#3) 17-18-19 (#4)		17-18-19 (#1) 17-18-19 (#2) 17-18-19 (#3) 17-18-19 (#4)		17-18-19 (#1) 17-18-19 (#2) 17-18-19 (#3) 17-18-19 (#4)		17-18-19 (#1) 17-18-19 (#2) 17-18-19 (#3) 17-18-19 (#4)	

D. Supplementary Case Studies

In order to demonstrate how natural gas transmission constraints and MG operations affect the scheduling of SR in coordinated electricity and natural gas networks, four cases are provided.

TABLE II
RESULTS OF SR PROBLEM IN FOUR CASES

Decision Under Uncertainty	Case 1		Case 2		Case 3		Case 4	
	objective function	Lines opened	objective function	Lines opened	objective function	Lines opened	objective function	Lines opened
ADRO	6831.6	T2-T3-T4 (#1) T1-T2-T3 (#2) T1-T2-T3 (#3) T1-T2-T3 (#4)	5984.1	T2-T3-T4 (#1) T1-T2-T3 (#2) T1-T2-T6 (#3) T2-T3-T4 (#4)	7120.8	T2-T3-T4 (#1) T1-T2-T6 (#2) T1-T2-T6 (#3) T1-T2-T6 (#4)	6445	T2-T3-T4 (#1) T1-T2-T6 (#2) T1-T2-T6 (#3) T1-T2-T6 (#4)
Adaptive RO	6567.1	T2-T3-T4 (#1) T2-T3-T4 (#2) T1-T2-T6 (#3) T2-T3-T4 (#4)	5771.1	T2-T3-T4 (#1) T1-T2-T6 (#2) T2-T3-T4 (#3) T1-T2-T3 (#4)	6970.8	T1-T2-T3 (#1) T1-T2-T6 (#2) T1-T2-T3 (#3) T1-T2-T6 (#4)	6239.5	T1-T2-T3 (#1) T1-T2-T3 (#2) T1-T2-T6 (#3) T1-T2-T6 (#4)
Two-Stage Stochastic Programming	8494.7	T1-T2-T3 (#1) T2-T3-T4 (#2) T1-T2-T6 (#3) T2-T3-T4 (#4)	7596.1	T1-T2-T6 (#1) T2-T3-T4 (#2) T1-T2-T3 (#3) T2- T3-T4(#4)	8936.6	T2-T3-T4 (#1) T1-T2-T6 (#2) T1-T2-T3 (#3) T1- T2-T6(#4)	8231.9	T1-T2-T3 (#1) T1-T2-T6 (#2) T1-T2-T6 (#3) T1- T2-T3(#4)

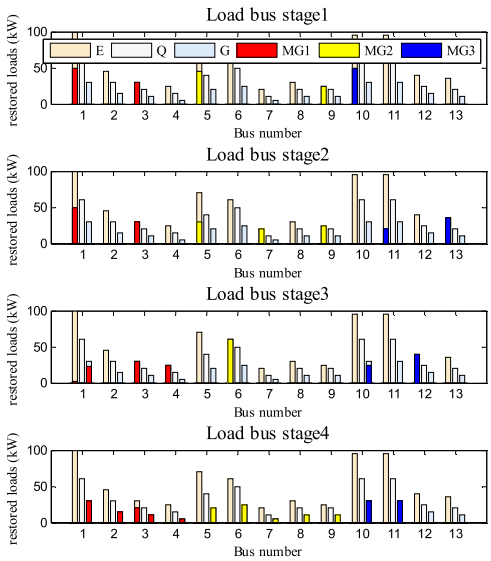

Fig. 9. Four-time step SR (kW) scheduling for $\beta = 3$ and $\omega = 4$.

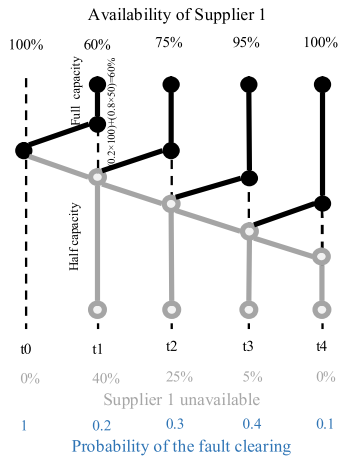

Fig. 10. Tree diagram related to the availability of supplier 1.

1) *Case 1:* Equal dispatch of natural gas between NGFGUs and deterministic injection of gas from supplier 1.
2) *Case 2:* Equal dispatch of natural gas between NGFGUs and stochastic injection of gas from supplier 1.
3) *Case 3:* Dispatching of natural gas between NGFGUs and deterministic injection of gas from supplier 1.
4) *Case 4:* Dispatching of natural gas between NGFGUs and stochastic injection of gas from supplier 1.

The simulation results of SR and the structure of MGs during the 4 h and four case studies are presented in Table II.

The tree diagram related to the availability of supplier 1 is shown in Fig. 10. In this figure, the possibility of fault clearing and connection to the upstream network is shown in 4 h with blue color. It is assumed that the compressor is affected and stopped during the fault. Thus, in the first hour, the probability of fault clearing is 0.2, and the availability of supplier 1 is equal to $0.2 \times 100\%$, the probability of fault presence is 0.8, and the availability with half capacity is equal to $0.8 \times 50\%$. The total availability in the first hour is obtained by $(0.2 \times 100) + (0.8 \times 50) = 60\%$.

In case 1, it shows that the result of ADRO is 4% more and 19% less than the result of ARO and SP, respectively. Considering the solution of the ARO, it is concluded that the solution of the ADRO protects the optimal schedule of SR against 4% loss. While the SR problem can gain 19% with the SP approach, it can still suffer a large loss if it is implemented. Due to the reduction of the availability of supplier 1 in case 2, it can be seen that the objective function of ADRO is reduced by 14% compared to case 1. This also happens 13% and 11% for ARO and SP, comparison to case 1, respectively.

As shown in Table I, ADRO has increased by about 5% compared to case 1 and by about 20% compared to case 2. Also, the objective function has increased for ARO and SP compared to case 1 and case 2. This shows the importance of the dispatching capability in the gas supply network in order to achieve the optimal response. By comparing the results, ADRO in case 4 is 6% less and 8% more than case 1 and case 2, respectively. Also, it is 10% less than the result of case 3. This shows the importance of a reliable supply of natural gas for NGFGUs. The production of NGFGUs and engine generators embedded in PHEVs, as well as the power exchange of EVs' battery in each of the formed MGs, and the amount of restored loads in case 4 are presented in Fig. 11. Comparing the total production in each MG with the SR shows that the power balance constraint has been established.

In case 4, the operation detail in 4 h until clearing the fault is presented in Fig. 12. This figure shows the production of NGFGUs, power exchange of EVs (green), load restoration (E,Q,G) in kilowatt, and switching program in each step.

By analyzing the results for ADRO, it is clear that in the first hour, due to the low importance and weight coefficient of loads, the restoration value is zero. It shows the importance of dynamic programming instead of step-by-step solution to get

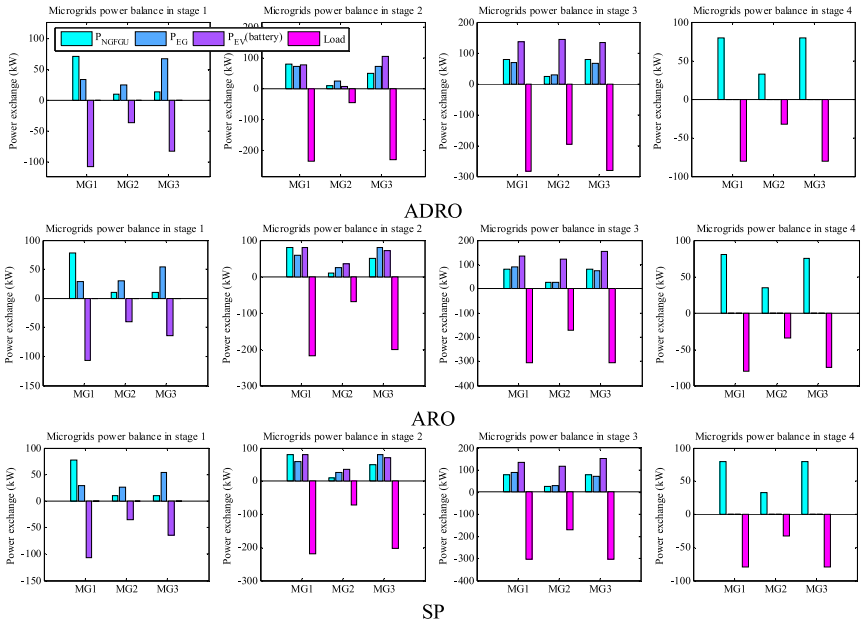

Fig. 11. Power exchange program in each SR model.

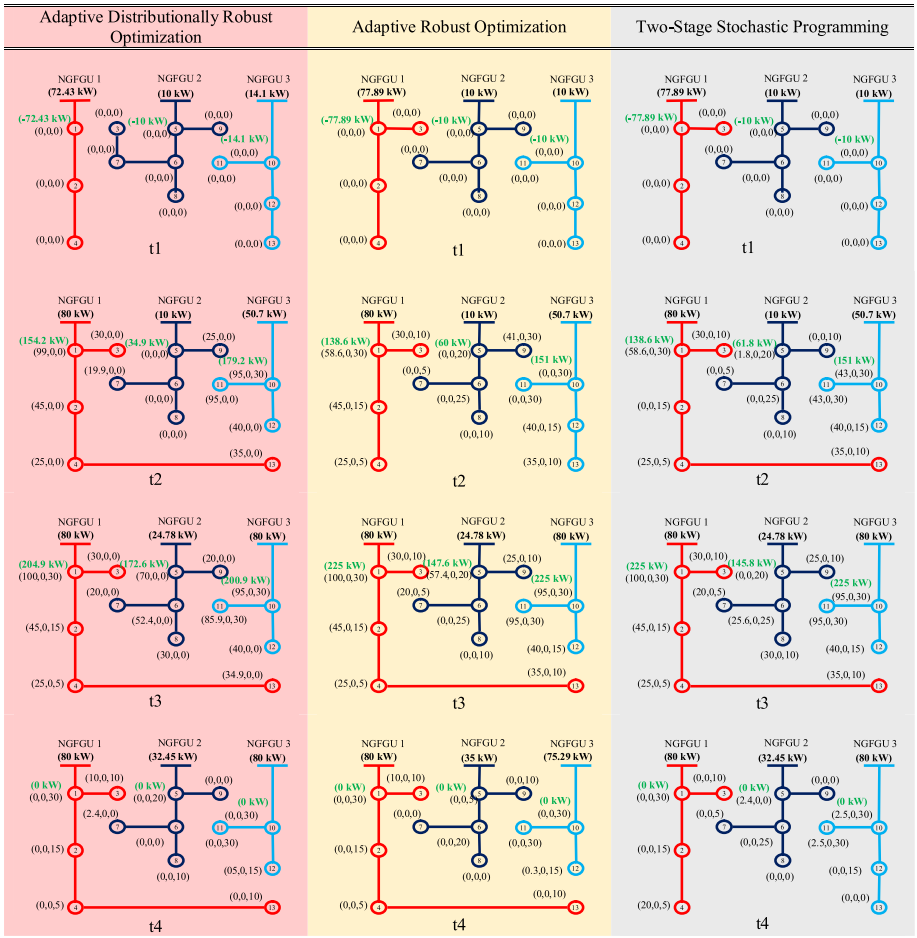

Fig. 12. Optimal operation and SR program in self-healing mode [NGFGU generation: Bold, PHEV power exchange: Green and restored load in each bus: (E,Q,G)].

TABLE III
SR IN EACH MG AND FOUR TIME STEPS IN THREE OPTIMIZATION METHODS

Decision Under Uncertainty		ADRO (CVaR)	Adaptive RO	Two-Stage Stochastic Programming
		$\sum \lambda \times P$		
MG1	t 1	0	0	0
	t 2	3864.5	3458.1	3433.1
	t 3	3393.3	3613.5	3613
	t 4	1150	1150	1115
MG2	t 1	0	0	0
	t 2	742.29	980	1010.3
	t 3	2389.3	2009.7	1987.4
	t 4	474.5	525	474.5
MG3	t 1	0	0	0
	t 2	3795	3117.6	3142.6
	t 3	3334	3608	3608
	t 4	1175	1128	1175

more comprehensive results. In the first hour, all the production of the NGFGUs is used to charge the batteries of EVs to be used in the next hours.

By comparing the results of ADRO with ARO and SP in Fig. 12, it is clear that there is a unique structure and SR program during the fault period for each of the methods, and the decision maker can select both planning decisions to ex-ante preventive actions and operation decisions to ex-post correction actions, based on his/her criteria.

The details of the optimization response and SR in the worst scenario ($\omega = 4$) are presented in Table III. It shows that in all three optimization methods, the amount of load restored in the first hour is zero. Fig. 12 illustrates how the power generated by the generators in the first hour is used to store energy for load restoration in the next hours. Table III also demonstrates that the optimization methods are effective in optimal load restoration over time and comprehensive results. This highlights the importance of strategic energy management in using a global optimization instead of using a step-by-step optimal solution for successful SR in emergency scenarios.

Furthermore, for each of the three MGs, Table III presents the optimal response of the hourly product of load in the important coefficient $(\sum \lambda_E \times P_E + \lambda_Q \times P_Q + \lambda_G \times P_G)$.

Thus, according to the highlighted better responses, it is proven that using each method, it is possible to obtain a superior optimal response for a specific period. However, it is important to choose a problem-solving method for the entire operational period.

In Table IV, the optimization response for each scenario in each of the problem-solving methods is presented. A detailed analysis of the characteristics of the optimal points as well as the final decision of each method is described in this table. This analysis allows decision-makers for a comparison of the effectiveness of each problem-solving method in addressing the scenarios presented. By examining the optimization output of each method, insights can be gained into which approach may be most suitable for different types of optimization problems.

By analyzing the results, it is clear that the standard deviation of the optimization results for different scenarios in ADRO is equal to 27.5%. This value is the lowest standard deviation compared to ARO and SP with 35.6% and 36.01%, respectively. The lowest standard deviation at ADRO can be considered an important advantage because decision-makers can take decisions with greater confidence when faced with different scenarios.

TABLE IV
OPTIMIZATION RESULT FOR EACH SCENARIO IN EACH STATISTICAL COMPARISON OF RESULTS

Decision Under Uncertainty	ADRO (CVaR)	Adaptive RO	Two-Stage Stochastic Programming
Cplex time (s)	0.33	0.27	0.5
ω1	6756.6	7420.4	7564.6
ω2	6444.6	6555.9	6700.6
ω3	6605.6	6758.9	6869.1
ω4	6447.1	6239.4	6347.6
ω5	8239.7	8544.2	8748.7
ω6	8062.9	8016.7	8195.2
ω7	8255.8	8892.2	9076.2
ω8	7971.9	7816.7	7942.7
ω9	8895.5	9743.5	9920.4
ω10	8743.5	9107.0	9253.9
ω11	8781.5	9158.5	9339.9
ω12	8667.5	8672.5	8823.9
Objective function	**6445**	**6239.5**	**8231.9**
Deviation of the scenarios	27.5%	35.6%	36.01%
Average of the scenarios	7822.7	8077.2	8231.9

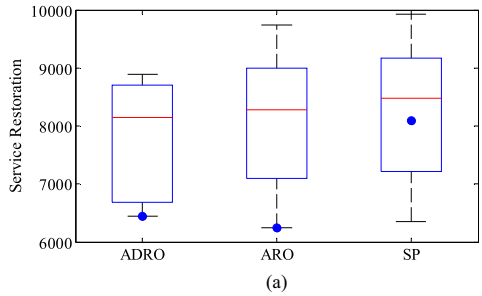

Fig. 13. Optimization solution box plots for three approaches to problem solving.

Another advantage of ADRO compared to ARO is that, despite adopting a robust approach to decision-making and despite the lower standard deviation compared to ARO, it reaches better optimal results than ARO with a value of 6445 compared to 6239.5. The high value of the objective function in SP, with 8231.9, and the highest standard deviation, with 36.01%, while making decision-making challenging, also has a high risk of losses and damage from exposure to undesirable scenarios. Therefore, ADRO provides a more reliable and efficient solution for decision-making in comparison to both ARO and SP. By minimizing risk and maximizing optimal results, ADRO proves to be a superior approach in complex scenarios.

Fig. 13 displays box plots of optimization problem solution approaches for graphical analysis purposes. The box shows the interquartile range (IQR), while the whiskers indicate the data range defined as 1.5×IQR. The median is represented by the horizontal line within each box, and the circle represents the position of the objective function's output.

In the tree optimization problems, the box plots show how the center and spread of optimal scenario profits have been distributed to inform decisions based on statistical analysis. A robust response is provided by ADRO and ARO, as shown by the position of the ideal response point on the lower whisker in Fig. 13, where an increase in the distance between the whiskers indicates an increase in the standard deviation.

It shows that the distribution of the optimal SR results for ADRO, ARO, and SP has an increasing trend from 27.5% to

36.01%, as shown in Table IV. It should be noted that risk-averse solutions are indicated by comparatively low profit standard deviation values and high objective function values.

V. Conclusion

In this article, a coordinated model of natural gas network and electric power system is proposed for SR problems in self-healing mode. By employing advanced optimization techniques such as ADRO and SP, the study not only maximizes SR but also equips decision-makers with the tools to navigate the complexities of uncertain operational parameters effectively. To evaluate the results, ADRO is analyzed in several case studies. In case 4, it is 6% less and 8% more than case 1 and case 2, respectively. Also, it is 10% less than the result of case 3. This shows the importance of a reliable supply of natural gas for NGFGUs. According to the results, it is clear that after the reliable supply of natural gas, the dispatching capability of the gas network is the second priority to reach the best optimal response. Furthermore, by comparing the outcome of ADRO with that of ARO and SP, the decision-maker can conclude the following bullets.

1) All three optimization methods show zero load restoration in the first hour, highlighting the importance of strategic energy management.
2) The standard deviation of optimization results for different scenarios in ADRO is 27.5%, the lowest compared to ARO and SP.
3) ADRO provides a more reliable and efficient solution for decision-making compared to both ARO and SP.
4) Box plots of optimization problem solution approaches are displayed for graphical analysis.
5) The distribution of optimal scenario profits for ADRO, ARO, and SP shows an increased trend from 27.5% to 36.01%; so, risk-averse solutions are indicated by comparatively low profit standard deviation values and high objective function values.

References

[1] E. Litvinov, F. Zhao, and T. Zheng, "Electricity markets in the United States: Power industry restructuring processes for the present and future," *IEEE Power Energy Mag.*, vol. 17, no. 1, pp. 32–42, Jan./Feb. 2019.

[2] A. Zlotnik, L. Roald, S. Backhaus, M. Chertkov, and G. Andersson, "Coordinated scheduling for interdependent electric power and natural gas infrastructures," *IEEE Trans. Power Syst.*, vol. 32, no. 1, pp. 600–610, Jan. 2017.

[3] S. M. Mohammadi-Hosseininejad, A. Fereidunian, A. Shahsavari, and H. Lesani, "A healer reinforcement approach to self-healing in smart grid by PHEVs parking lot allocation," *IEEE Trans. Ind. Inform.*, vol. 12, no. 6, pp. 2020–2030, Dec. 2016.

[4] E. Shahryari, H. Shayeghi, B. Mohammadi-Ivatloo, and M. Moradzadeh, "Optimal energy management of microgrid in day-ahead and intra-day markets using a copula-based uncertainty modeling method," *J. Oper. Automat. Power Eng.*, vol. 2, pp. 86–96, 2019.

[5] H. Shayeghi and M. Alilou, "Multi-objective demand side management to improve economic and environmental issues of a smart microgrid," *J. Oper. Automat. Power Eng.*, vol. 9, no. 3, pp. 182–192, Dec. 2021.

[6] National Energy Technology Laboratory, "A systems view of the modern grid," 2007. [Online] Available: https://www.netl.doe.gov/, Accessed: 2018.

[7] R. E. Robert, M. P. Croissant, and J. R. Masih, "International energy outlook: U.S. department of energy," *Wash Quart*, vol. 19, no. 4, pp. 70–99, 1996.

[8] C. M. Correa-Posada and P. SáNchez-Martın, "Security-constrained optimal power and natural-gas flow," *IEEE Trans. Power Syst.*, vol. 29, no. 4, pp. 1780–1787, Jul. 2014.

[9] N. Afsari, S. J. SeyedShenava, and H. Shayeghi, "Chance constrained robust hydrogen storage management to service restoration in microgrids considering the methanation process model," *Int. J. Hydrogen Energy*, vol. 50, pp. 1463–1476, 2024.

[10] H. Khani and H. E. Z. Farag, "Optimal day–ahead scheduling of power–to–gas energy storage and gas load management in wholesale electricity and gas markets," *IEEE Trans. Sustain. Energy*, vol. 9, no. 2, pp. 940–951, Apr. 2018.

[11] Z. Yang, C. Gao, and J. Zhang, "The interaction of gas and electricity hybrid energy internet," in *Proc. IEEE Conf. Energy Internet Energy Syst. Integr.*, 2017, pp. 1–6.

[12] Y. Li et al., "Day-ahead schedule of a multi-energy system with power-to-gas technology," in *Proc. IEEE Power Energy Soc. Gen. Meeting*, 2017, pp. 1–5.

[13] X. Zhang, M. Shahidehpour, A. Alabdulwahab, and A. Abusorrah, "Hourly electricity demand response in the stochastic day-ahead scheduling of coordinated electricity and natural gas networks," *IEEE Trans. Power Syst.*, vol. 31, no. 1, pp. 592–601, Jan. 2016.

[14] L. Min, C. Lou, J. Yang, J. Yu, and Z. Yu, "Operational coordination optimization of electricity and natural gas networks based on sequential symmetrical second-order cone programming," *J. Modern Power Syst. Clean Energy*, vol. 13, no. 2, pp. 488–499, Mar. 2025.

[15] P. Sunday Onen, R. H. A. Zubo, N. T. Ali, G. Mokryani, J. -P. Li, and R. Abd-Alhameed, "Stochastic expansion planning model for a coordinated natural gas and electricity networks coupled with gas-fired generators, power-to-gas facilities, and renewable power," *IEEE Access*, vol. 12, pp. 105811–105830, 2024.

[16] M. Jadidbonab, H. Abdeltawab, and Y. A. -R. I. Mohamed, "An optimal routing framework for an integrated urban power–gas–traffic network," *IEEE Open J. Intell. Transp. Syst.*, vol. 5, pp. 223–237, 2024.

[17] M. R. Bussieck and A. Pruessner, "Mixed-integer nonlinear programming," *SIAG/OPT Newsl. Views News*, vol. 14, pp. 19–22, 2003.

[18] H. Shin and R. Baldick, "Plug-in electric Vehicle to Home (V2H) operation under a grid outage," *IEEE Trans. Smart Grid*, vol. 8, no. 4, pp. 2032–2041, Jul. 2017.

[19] H. Momen, A. Abessi, S. H. Jadid, M. Shafie-khah, and J. Catalao, "Load restoration and energy management of a microgrid with distributed energy resources and electric vehicles participation under a two-stage stochastic framework," *Int. J. Elect. Power Energy Syst.*, vol. 133, Dec. 2021, Art. no. 107320.

[20] N. Afsari, S. J. Seyedshenava, and H. Shayeghi, "A MILP model incorporated with the risk management tool for self-healing oriented service restoration," *J. Oper. Automat. Power Eng.*, vol. 12, no. 1, pp. 1–13, 2022.

[21] H. Zhu et al., "Robust post-disaster repair crew dispatch for distribution systems considering the uncertainty of switches," *Int. J. Elect. Power Energy Syst.*, vol. 155, 2023, Art. no. 109550.

[22] G. Li, R. Zhang, T. Jiang, H. Chen, L. Bai, and X. Li, "Security-constrained bi-level economic dispatch model for integrated natural gas and electricity systems considering wind power and power-to-gas process," *Appl. Energy*, vol. 194, pp. 696–704, 2017.

[23] J. R. Birge and F. Louveaux, *Introduction to Stochastic Programming*, 2nd ed. New York, NY, USA: Springer-Verlag, 2011.

[24] D. Bertsimas, D. B. Brown, and C. Caramanis, "Theory and applications of robust optimization," *SIAM Rev.*, vol. 53, no. 3, pp. 464–501, 2011.

[25] A. Bagheri, J. Wang, and C. Zhao, "Data-driven stochastic transmission expansion planning," *IEEE Trans. Power Syst.*, vol. 32, no. 5, pp. 3461–3470, Sep. 2017.

[26] E. Delage and Y. Ye, "Distributionally robust optimization under moment uncertainty with application to data-driven problems," *Oper. Res.*, vol. 58, no. 3, pp. 595–612, 2010.

[27] X. Sun and A. J. Conejo, *Robust Optimization in Electric Energy Systems*. New York, NY, USA: Springer-Verlag, 2021.

[28] N. Afsari, S.J. S.Shenava, and H. Shayeghi, "Self-healing policy in distribution network considering technical indices," in *Proc. Smart Grid Conf.*, 2019, pp. 1–6.

[29] A. J. Conejo, M. Carrión, and J. M. Morales, *Decision Making Under Uncertainty in Electricity Markets*. New York, NY, USA: Springer-Verlag, 2010.

[30] M. Zadsar, M.R Haghifam, and S.M Miri, "Approach for self-healing resilient operation of active distribution network with microgrid," *IET Gener., Transmiss. Distrib.*, vol. 11, no. 18, pp. 4633–4643, 2017.

[31] B. Zhao, X. Dong, and J. Bornemann, "Service restoration for a renewable-powered microgrid in unscheduled island mode," *IEEE Trans. SMART GRID*, vol. 6, no. 3, pp. 1128–1136, May 2015.

[32] 2015. [Online]. Available: motor.ece.iit.edu/data/Gastranssmion6_1.xlsx